Waveguiding and frequency selection of Lamb waves in a plate with a periodic stubbed surface

Tzung-Chen Wu, Tsung-Tsong Wu,* and Jin-Chen Hsu
Institute of Applied Mechanics, National Taiwan University, Taipei 106, Taiwan
(Received 9 November 2008; revised manuscript received 6 February 2009; published 30 March 2009)

In this paper, we numerically and experimentally study the waveguiding of Lamb modes in a thin plate with a periodic stubbed surface and propose a frequency-selection method based on the found complete band gaps of Lamb waves in the periodic structure. In the numerical simulations, we employ finite-element method to analyze the waveguiding effect of a line defect created in the periodic plate structure; and on the experimental side, we utilize a pulsed laser to generate broadband elastic-wave energy and a laser interferometer to receive the wave signals inside the line-defect waveguide. In the experiment, well-confined acoustic energy in the acoustic band gaps is observed. Furthermore, a polyline sharply bent waveguide is designed and used for the frequency selection of Lamb waves. Measurements show that acoustic energy with frequencies in the band gaps can be separated out and guided by the bent waveguiding route. The characteristics of deaf bands found in the experiment are discussed as well.

DOI: 10.1103/PhysRevB.79.104306 PACS number(s): 43.35.+d, 42.62.−b, 63.20.−e, 46.40.Cd

I. INTRODUCTION

Over the last decade, propagation of bulk and surface acoustic waves in the periodic structures called phononic crystals (PCs) has attracted a lot of interests due to their renewed physical properties.[1–11] The existence of band gaps, the frequency ranges in which acoustic-wave propagation is forbidden, in such periodic structures has led to a variety of potential applications, such as filters, efficient acoustic waveguides, etc.[12,13] Moreover, several studies related to the propagation of Lamb waves in plate structures comprised of PCs have been presented recently. On considering the so-called phononic-crystal plates, the frequency band structure of acoustic waves propagating in the plates composed of two different kinds of solid constituents periodically arranged have been studied numerically[14,15] and experimentally.[16] The released results showed that in addition to the filling factor, the ratio of the slab thickness to the lattice period is a key parameter to the existence of complete band gaps. Specifically, Bonello *et al.*[17] investigated Lamb wave modes in a silicon plate coated with a very thin two-dimensional (2D) phononic film and found the appearance of ministop bands at the edges of the first and second Brillouin zones by means of laser ultrasonic technique. Instead of coating thin film on plates, Lamb waves in a plate with an engraved periodic grating were investigated by Morvan *et al.*[18] For higher-frequency demonstration, Mohammadi *et al.*[19] experimentally resolved the high-frequency gaps created by a microstructure of periodical cylindrical air holes in a silicon plate. In a recent paper, Wu *et al.*[20] numerically and experimentally demonstrated the existence of complete band gaps and resonant characteristics in a plate with a periodic stubbed surface. The investigation shows that a complete band gap is opened up as the height of the stubs increases up to about triple the plate thickness, and the energy can be trapped in the resonant stubs on the plate surface. On the other hand, some features of low-frequency gaps in similar structures were also proposed simultaneously.[21]

Based on the complete frequency band gaps of acoustic waves in the structure proposed in Ref. 20, we further investigate the waveguiding effect in the plate with a periodic stubbed surface and apply the effect to design a defect-contained structure for frequency selection of Lamb waves in this paper. Sections II–V are organized as follows. First, detailed evolution of the complete band gaps and the propagation of guided modes in the stubbed phononic plate with a line defect are discussed and studied numerically using the finite-element (FE) method with the COMSOL MULTIPHYSICS program.[22] Next, the laser ultrasonic experiments are accordingly conducted to demonstrate the guiding effect on Lamb waves in the line-defect PC structure. Then based on the effect, a design for the frequency selection of Lamb waves in the PC with a polyline waveguide is proposed; furthermore, measured results of the frequency selection by using laser ultrasonic techniques are presented. Finally, some conclusions are given.

II. FORMATION OF BAND GAPS IN A THIN PLATE WITH A PERIODIC STUBBED SURFACE

In this section, the evolution of the band gaps in a thin plate with a periodic stubbed surface is studied first by gradually increasing the height of the stubbed cylinders. Consider a thin plate (plate thickness of $h_1=1$ mm) with periodic cylindrical stubs on one of the plate surfaces [a unit cell of the structure is shown in Fig. 1(a)]. The material

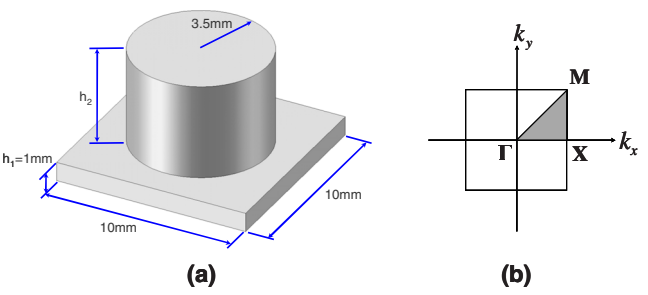

FIG. 1. (Color online) (a) Schematic of a unit cell of the PC plate with a periodic stubbed surface and (b) the corresponding first Brillouin zone. Gray area in (b) is the irreducible part of the zone.

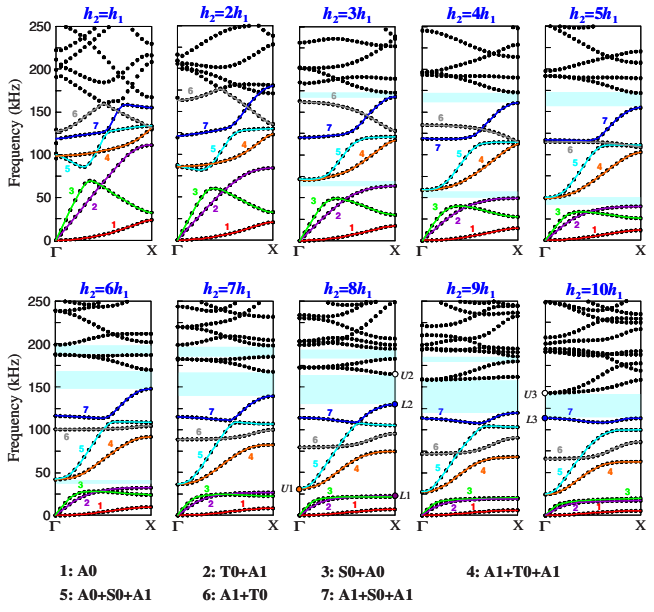

FIG. 2. (Color online) Variations in dispersion curves along the Γ-X direction with increasing stub height. The frequency ranges with shade (in blue color) denote the complete band gaps.

chosen to constitute the whole structure is aluminum 6061.[23] The cylindrical stubs are arranged in square lattice with a lattice constant $a=10$ mm. The diameter of the cylindrical stubs is $d=7$ mm and the filling factor defined as $F=\pi d^2/4a^2$ is 0.385. For waves propagating along the Γ-X direction in the first Brillouin zone [referring to Fig. 1(b)], the calculated dispersion relations are shown in Fig. 2. The height of the stubs increases from one time of the plate thickness (h_1) gradually up to $10h_1$. When the height of the stubs increases, some resonances are formed and thus result in slower wave velocity and flatter bands[20] near the edge of the Brillouin zone (i.e., at the X point). We note that as the stub height is about three times that of the plate thickness, i.e., $h_2=3h_1$, some narrow complete band gaps, the frequency ranges with shade in blue color in Fig. 2, start forming.

From Fig. 2, one can observe that as the stub height increases gradually, many bands originally crisscrossing in the dispersion curves start to separate at their intersections. The repelling of the bands finally results in different individual curves where each curve is composed of several evolved segments of old bands from the case of a uniform thin plate without the stubs. As a result of the repulsions, the mode coupling is resulted.[10] This evolution due to the existence of the stubs on the surface of the thin base plate makes the dispersion curves possess much more complicated vibrating modes. Each of these resulted modes in the dispersion curves could be composed of symmetric (denoted by S0, S1, etc.), antisymmetric (denoted by A0, A1, etc.), and transverse (denoted by T0, T1, etc.) vibrations or some of them. To be specific, the coupling modes of the lowest seven evolved dispersion curves and the evolution of the curves are identified in Fig. 2. These coupling modes can be considered as quasimodes related to several of the plate modes in the uniform thin plate. For example, the band labeled with the number 2 is transformed from the T0 and A1 modes of the uniform thin plate.

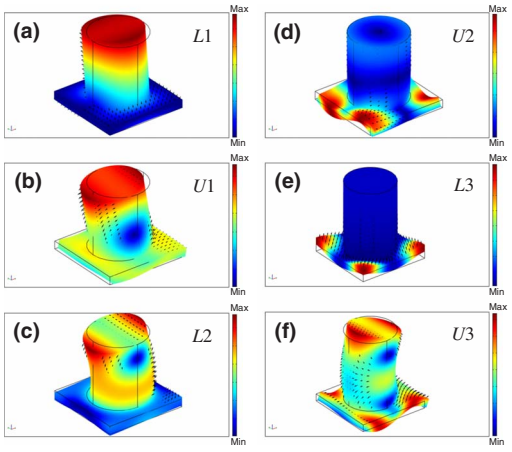

FIG. 3. (Color online) Displacement fields of several gap-edge modes at the points $L1$, $U1$, $L2$, $U2$, $L3$, and $U3$ labeled in Fig. 2.

Moreover, Fig. 2 also shows that the dispersion curves are getting flatter and flatter as the stub height increases. This effect could be explained by that the growth of the stubs on the plate causes the resonance that induces the flat bands because the acoustic energy is trapped by the periodic stubs. The phenomenon of energy trapping by periodic array of mechanical resonators had been shown in the surface wave propagation.[24] Increasing the height of the stubs lowers the resonant frequencies and enhances the mutual repelling of the bands. As a result, the band gaps are opened up and then widen. Specifically, as the stub height h_2 is equal to $9h_1$, the width of the complete band gap is the largest, which ranges from 119 to 157.5 kHz with a relative gap width equal to 27.8%. Note that when h_2 is smaller and between the values $3h_1$ and $6h_1$, the lowest band gaps connecting to the low-frequency ranges are opened up as complete band gaps rather than partial band gaps.[21] When the stub height is further increased to ten times of the thickness of the base plate, i.e., $h_2=10h_1$, a complete band gap appears from 114 to 143 kHz, and three partial band gaps appear at the same time, as shown in the final plot of Fig. 2. To give more intuitive understanding of the band-gap formation, the displacement fields of eigenmodes at several gap-edge frequencies marked in Fig. 2 (the points $L1$, $U1$, $L2$, $U2$, $L3$, and $U3$) are plotted in Fig. 3 to show how the stub height influences the evolution of the dispersion curves. Figure 3(a) shows the displacement field of $L1$ mode at the bottom-edge frequency of the first gap. This field displays significant vibrations concentrated in the stub that behave as a lower-order bending wave in a cantilever beam. It can be observed that the stub height associates with quarter wavelength of the bending mode. Therefore, when the stubs are taller, the eigenfrequency of $L1$ mode becomes lower. From Fig. 2 with the variation in stub height h_2, a simple approximate relation between the stub height and the eigenfrequency of the bottom-edge mode $L1$ of the first gap can be given by $f_{L1}h_2=190$ m/sec. The displacement field of the $U1$ mode at the upper-edge frequency of the first gap shown in Fig. 3(b) has similar characteristics to $L1$ mode, but the stub motion accompanies bending with some twisting vibration. Similarly, the approximation $f_{U1}h_2=245$ m/sec can be arrived. Moreover, the dis-

placement fields of the gap-edge modes $L2$ and $U3$ shown in Figs. 3(c) and 3(f) also have obvious vibrations concentrated in the stubs; their eigenfrequencies, therefore, are inversely proportional to the stub height. The formation of the band gaps relies on the resonance of the stubs to induce the flat low-lying bands. On the other hand, the gap-edge modes $U2$ and $L3$ exhibit very different characteristics. From Figs. 3(d) and 3(e), the displacement fields of $U2$ and $L3$ modes show that the vibrations are mostly localized in the thin plate, and the stubs remain almost vibrationless. As a result of the vibrationless stubs in $U2$ and $L3$ modes, changes in the stub height will not significantly influence the values of the eigenfrequency of $U2$ and $L3$ modes.

The case of the structure with $h_2=10h_1$ is of interest and considered eventually in our experiment by two reasons. (1) Three partial band gaps along the Γ-X direction in this case are found. With these additional partial band gaps, the phenomenon of band gaps can be expressed more evidently. (2) A nearly flat band evolved from the antisymmetric and symmetric ($A1$ and $S0$) modes[20] with frequency around 110 kHz is found between two band gaps; the modes of this nearly flat band may result in obvious resonances and are expected to be measured in experiment. The full picture of dispersion relations for this structure calculated along the boundaries of the corresponding irreducible first Brillouin zone (i.e., along Γ-X-M-Γ) can be seen on Fig. 2 of Ref. 20.

In Ref. 20, the experimental characterizations of the band gaps for this structure by using the laser ultrasonic techniques showed that acoustic energies with frequencies in the complete and partial band gaps exhibit much lower intensities in the measured spectra which agree well with the numerical result (Fig. 2 of Ref. 20) and correspond to the fact that Lamb waves with frequencies in the gaps attenuate during the propagation. In addition, some resonant peaks appearing at some of the band-edge frequencies, such as at 19 (the bottom edge of the first partial band gap), 100, and 109 kHz (the bottom and upper edges of the second partial band gap, respectively), where the slopes of the frequency bands approach zero which associate with high density of states of Lamb modes, were observed. In addition, the eigenmode analysis by FE method also showed that there exist strong vibrations either in the base plate or in the stubs at these frequencies where the resonant peaks appear. Moreover, a frequency range (about 66–100 kHz) in the measured spectra corresponding to no band gaps and exhibiting low intensity was also found. The frequency bands in this range are referred to as the deaf bands due to ineffective excitation of the modes by the given source.

III. STRAIGHT WAVEGUIDE

Based on the measurement of the complete band gap in the plate with a periodic stubbed surface demonstrated in Ref. 20, a further application to 2D guiding structure for Lamb waves is conducted and investigated by numerical calculations and laser ultrasonic experiments[25,26] in this section. In the numerical study, a line-defect waveguide produced by removing one row of the stubs from the perfect periodic structure is considered. The geometrical parameters of the

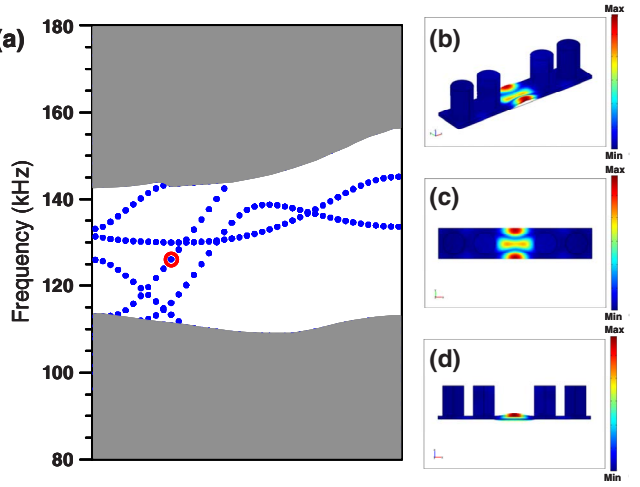

FIG. 4. (Color online) (a) Band structures along the Γ-X direction for the phononic crystal containing a waveguide produced by removing one row of the stubs. The waveguide is considered as 1×5 supercell in the y direction with the line defect along the x direction. (b)–(d) are the eigenmode shapes corresponding to the red circle marked in (a) with different viewpoints, respectively.

defect-contained structure are the same as the scales considered in the final plot of Fig. 2 (i.e., $a=10$ mm, $h_1=1$ mm, $d=7$ mm, and $h_2=10$ mm) but one row of the stubs has been removed. To execute the numerical calculation, a FE structural model containing five unit cells, referred to as a 1×5 supercell, is set up, where the stub in the third unit cell is removed in the model [see Fig. 4(b)]. Then by applying the Bloch periodic boundary conditions to the 1×5 supercell model, the frequency band structure is obtained and shown in Fig. 4(a). In the figure, it can be clearly observed that some additional frequency bands, which correspond to the existence of defect modes localized in the waveguide, appear inside the complete band gap. Specifically, consider the defect mode with frequency in the complete band gap marked by the red circle in Fig. 4(a) with the reduced wave number $ka/\pi=0.25$ and frequency $f=126$ kHz. The intensity of the displacement field of the mode is plotted in Figs. 4(b)–4(d) from three different views, respectively. In these figures, it is obvious that most of the elastic-wave energy is well confined within the area of the line-defect waveguide.

To confirm the feasibility of the waveguiding of Lamb waves experimentally, a real PC thin plate with a stubbed surface containing a line-defect waveguide is manufactured by a mechanical machining process. In the experiment, measurements are in the straight waveguide and the receiver (laser interferometer) is five rows apart from the source (applied by Nd:YAG pulsed laser). The scales of the phononic unit cell in the realized structure are the same as that considered in the model of the numerical calculations, i.e., $a=10$ mm, $h_1=1$ mm, $d=7$ mm, and $h_2=10$ mm, and the structure is made of aluminum 6061. Also, the machining process for the structure with a maximal fabrication tolerance of less than 50 μm is achieved, and the edges of this experimental specimen are extensive enough to avoid the influence of the reflected wave from the boundaries. Figure 5 shows the experimental reference spectrum, which is defined as the

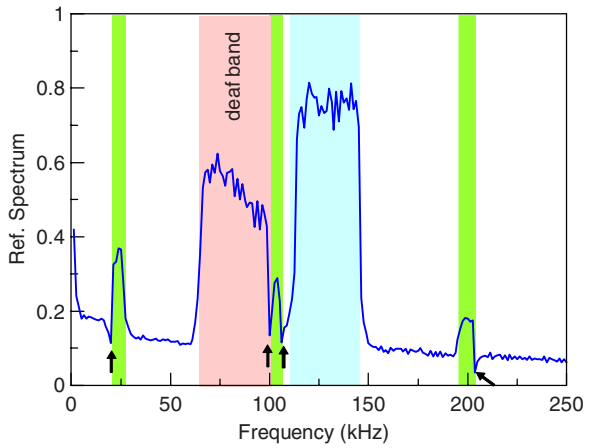

FIG. 5. (Color online) Measured reference spectra for the waves propagating in the PC plate structure with the straight waveguide.

ratio of the spectrum measured on the defect-contained stubbed PC plate to that measured on a uniform plate with thickness equal to 1 mm. The digitized sampling rate for the signal from the interferometer is 50 MHz so the spectrum in good resolution is obtained. In the figure, the frequency ranges in blue and green colors are, respectively, corresponding to the complete and partial band gaps of the perfect structure without the defect. From the figure, it can be observed that the acoustic energy with frequency in the complete band gap is well confined to propagate in the waveguide so that the high-intensity spectra in the gap are received in the measurement. Also, the confinement of the energies within the three partial band gaps in the Γ-X direction is obtained in the spectrum. As a result of the experiments, the measured spectrum agrees very well with the numerical prediction about the band gaps. By contrast, for the waves with frequencies not in the band gaps, the energy could freely radiate out without effective blocking by the band-gap effect. It is worth noting that in Fig. 5, there are four arrows that indicate four points of relatively low intensities in the reference spectrum. The locations of these four frequencies are at 20, 100, 110, and 205 kHz, which totally match the values of the resonant frequencies measured in Ref. 20. This special phenomenon can be explained by the reason that acoustic energies in the resonant frequencies are trapped and localized inside the phononic structure on the way to the receiver during the propagation along the waveguide. As a result, only very little acoustic energies may propagate through the waveguide when their frequencies are the same as the frequencies of resonance, and thus, the relatively low intensities at those frequency values resulted in the measured reference spectrum. In addition, in Fig. 5, the measured spectrum exhibits a range of high intensity (the pink region), corresponding neither to the complete band gap nor to the partial band gaps. This frequency range shows the location of the deaf band associated with this acoustic-wave generation by the pulsed laser and will be further discussed at the end of Sec. IV.

IV. POLYLINE BENT WAVEGUIDE

Since the Lamb waves with frequencies in the band gaps can only propagate along the line defect, i.e., the straight waveguide, one can make a channel based on the stubbed PC plate to control or guide the energy flow of the waves two dimensionally if the band gap is complete or omnidirectional. In this section, a design of a bent waveguide created in the PC plate used for frequency selection of Lamb waves is proposed, and results of laser ultrasonic measurement are demonstrated. The bent waveguide is formed with two-graduation turns produced by removing some of the stubs from the PC plate, and the schematic of the designed and fabricated structure is shown in Fig. 6. In the specimen, in order to avoid the influence of the reflected waves on the measured reference spectrum, some additional protruded thin-plate regions around the waveguide structure are reserved. To clearly explain the idea of designing this special waveguide, one can refer to Fig. 6(a) where when broadband elastic waves are generated in the thin plate, all the waves with frequencies either outside or inside the complete band gap are incident. It may be properly judged that most of the energy of those waves with frequencies outside the complete band gap may propagate straightforwardly through the phononic plate structure; however, for the waves with frequencies inside the complete band gap, the traveling acoustic energy cannot keep going straight because there are no allowed propagating modes for the wave to propagate into the stubbed regions. The incident waves are, therefore, compelled to make a turn and propagate along the polyline bent waveguide. Based on this simple prediction, it is encouraging to study this phenomenon experimentally.

For comparison, measurements of the ultrasonic signals are carried out at points **a**, **b**, **c**, and **d**, respectively, shown in Fig. 6(b). Note that the spectrum measured at point **a** (55 mm apart from the source) is a broadband signal that covers well

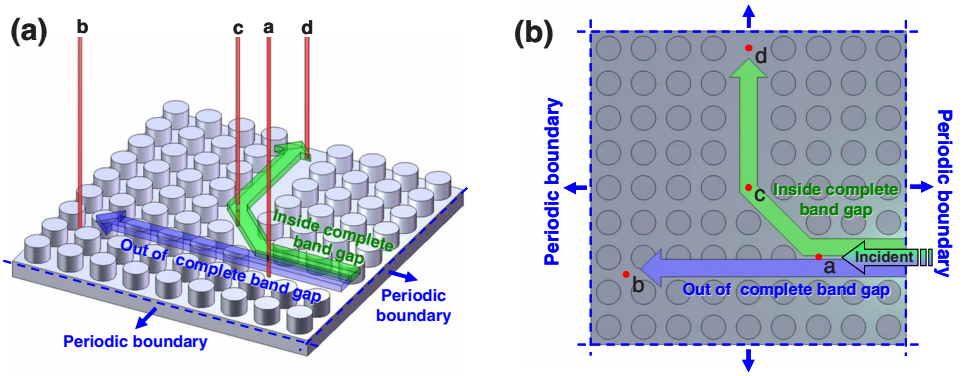

FIG. 6. (Color online) (a) Paths of the waves with frequency, respectively, outside and inside the complete band gap propagating in the structure with a bent waveguide. (b) Schematic of the waveguide experiment. Signals are received at points **a**, **b**, **c**, and **d**.

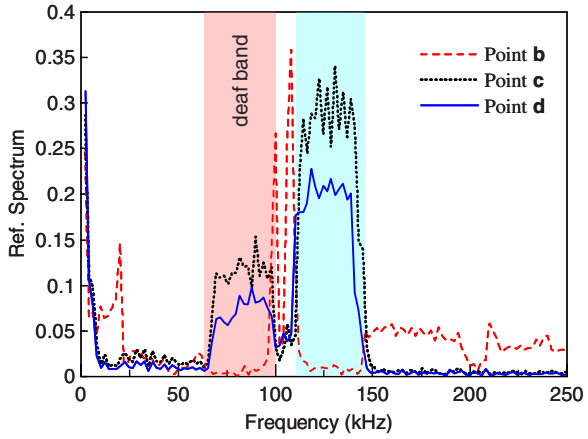

FIG. 7. (Color online) Comparison among the spectra measured at points **b**, **c**, and **d**.

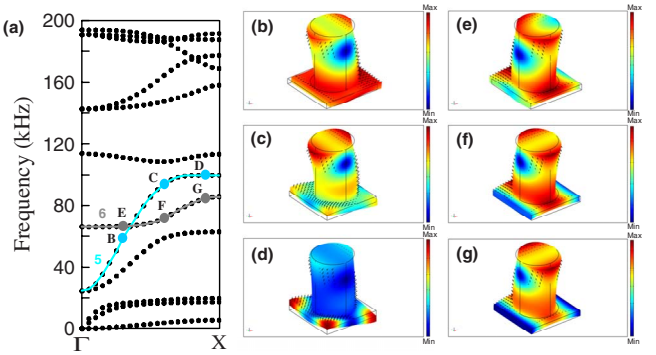

FIG. 8. (Color online) (a) Several eigenmodes of the deaf bands in the band structure. (b) Mode B with $f=58$ kHz, (c) mode C with $f=93$ kHz, (d) mode D with $f=100$ kHz, (e) mode E with $f=66$ kHz, (f) mode F with $f=71$ kHz, and (g) mode G with $f=84$ kHz. Modes B–D are in band 5 and modes E–G are in band 6.

the frequency range below 250 kHz so it is regarded as the reference corresponding to the measurements at other points (i.e., the points **b**, **c**, and **d**) in the following.

Figure 7 shows the reference spectra of the measurements at points **b** (red dashed line), **c** (black dotted line), and **d** (blue solid line), where the reference spectrum is defined as the ratio of the spectrum measured at the considered point to that measured at point **a**. For the measurement at point **b**, which is 60 mm apart from point **a**, the reference spectrum exhibits several peaks that associate with the resonance of the flat pass bands in the frequency band structure (the final plot in Fig. 2). Also, it can be observed that very low intensities are displayed in the ranges corresponding to the complete (from 114 to 143 kHz) and partial band gaps. Since the periodic stubs are ordered between points **a** and **b**, the measurement at point **b** is, therefore, intrinsically associated with the characteristics of waves in the perfect periodic structure (see Ref. 20). Now observe the spectra measured at point **c** and point **d** located inside the waveguide. An interesting phenomenon is found that in the band-gap frequency ranging from 114 to 143 kHz, the intensities of the spectra are obviously outstanding rather than sunken, with values of about 0.3 and 0.2. That is to say, the original broadband acoustic signals at point **a** are separated into the resonant energy with frequencies outside the complete band gap and guided energy within the complete band gap propagating along the bent waveguide. In other words, waves with frequencies outside the complete band gap may propagate straightforwardly, and waves with frequency within the complete band gap must propagate along the polyline bent waveguide. Based on the experimental results, we may conclude that the measured results conform to the prediction about the band-gap application schemed in Fig. 6(a), and the proposed phononic waveguide structure in the surface-stubbed plate may be characterized by the selection of acoustic frequency. On the other hand, an apparent attenuation can also be found, which may be due to the energy lost in causing the resonance of the periodic stubs or reflecting lost as turning. An optimized design of the bend of the waveguide could further enhance the guiding efficiency.

Furthermore, it should be noticed that in both Figs. 5 and 7 where the frequency range is marked in pink color (66–100 kHz), all the measured spectra in the waveguides exhibit an obviously higher intensity in the pink-color range which corresponds to no band gaps. However, an outstanding signal is still found in that region. To go a step further, this phenomenon is discussed in the following. On observing the band structure in Fig. 8(a) (a zoom in of the final plot of Fig. 2), there are two frequency bands (the bands 5 and 6) extended in the range from 66 to 100 kHz. Figures 8(b)–8(g) show the displacement fields of several eigenmodes in the two bands [modes of points B–G in Fig. 8(a)], where the arrows represent the displacement vectors of the particles. Modes B–D belong to band 5 which is composed of A0, S0, and A1 modes, and modes E–G belong to band 6, which is composed of A1 and T0 modes. For mode B with frequency $f=58$ kHz in band 5, the displacement field of the thin plate is almost a symmetric (S0) vibration. When the frequency increases along band 5, mode C with $f=93$ kHz and mode D with $f=100$ kHz show that the displacement fields of the base thin plate gradually transform from S0 vibration into antisymmetric (A0 and A1) vibrations. For modes E–G in band 6, all the displacement fields of the thin plate are almost a transverse (T0) vibration. In short, the eigenmodes are mainly governed by the vibrations associated with the symmetric (S0) and transverse (T0) plate modes in the frequency range above 66 kHz and below 100 kHz. However, the broadband elastic waves generated by the Nd:YAG pulsed laser are major in antisymmetric modes, minor in symmetric modes, and absent in transverse plate modes. Therefore, in Fig. 7, considering the frequency ranging from 66 to 100 kHz, the modes are not suitably coupling to and converted from the antisymmetric modes that can be effectively generated by the pulsed laser to propagate in the stubbed PC plate; therefore, most of the energy excited with frequencies in this range can only stay in the nonstubbed regions of the plate, i.e., the waveguides. As a result, for the laser ultrasonic excitation, this frequency range behaves as a complete band gap. In fact, modes in phononic-crystal structures which cannot be excited efficiently by some given source or incident waves are known as "deaf bands" and have once been found in the ultrasonic experiment on periodic solid-fluid composites by Hsiao *et al.*[27]. Based on the existence of the deaf band

with selectivity due to the applied source, it is reasonable to claim that waves with frequency ranging from 66 to 100 kHz should appear and be measured at points **c** and **d** in this experiment. Obviously, broadband signals can be separated into a lot of energy flows according to the wave properties in different frequency bands and can be measured at different positions through a proper design of the phononic structure.

V. SUMMARY AND CONCLUSIONS

In summary, we have demonstrated the formation of the band gaps in the plate with a periodic stubbed surface by discussing the evolution of the dispersion curves as the height of the stubs increase gradually. When the height of the stubs is three times greater than the plate thickness, complete band gaps forms, and when the stub height equals $9h_1$, the complete band gap is the largest. Based on the band gaps, the defect-contained stubbed PC plate structures with $h_2=10h_1$ are chosen to be manufactured, and then the guiding effect of Lamb waves inside a straight line-defect waveguide is experimentally studied using the laser ultrasonic technique. The measured results are in good agreement with the expectation about the confinement of energy of waves by the band-gap phenomenon. Also, the phenomenon of deaf band and the influence of the resonance can be identified clearly in the experiment.

As a result of the waveguiding, a phononic plate with a polyline defect that forms a sharply bent waveguide is designed and applied to use for frequency selection of Lamb waves. The characterizations of the selectivity of frequency are further conducted with experiments. The results show that energy in the desired frequency range (i.e., in the complete band gap) can be drawn out from a broadband signal based on the proposed design. That is, signals with the frequencies inside the complete band gap can be guided to follow the designed route and be detected at the exit of the waveguide. Moreover, acoustic energy in the deaf band associated with the given source can be controlled like those in the complete band gap. In other words, separation of the acoustic energy according to the ranges of the frequency by the structure is achieved. As a matter of fact, this sharply bent waveguide for frequency selection also provides an extra good method to examine the phenomenon of the deaf band. Finally, we note that the results of this paper could be further applied to innovative design of acoustic-wave devices.

ACKNOWLEDGMENT

The authors gratefully acknowledge financial support from the National Science Council of Taiwan (Grant No. NSC 96-2221-E-002-206-MY3).

*wutt@ndt.iam.ntu.edu.tw

[1] M. S. Kushwaha, P. Halevi, L. Dobrzynski, and B. Djafari-Rouhani, Phys. Rev. Lett. **71**, 2022 (1993).
[2] R. Sainidou, B. Djafari-Rouhani, and J. O. Vasseur, Phys. Rev. B **77**, 094304 (2008).
[3] Y. Tanaka and S. I. Tamura, Phys. Rev. B **58**, 7958 (1998).
[4] F. Meseguer, M. Holgado, D. Caballero, N. Benaches, J. Sánchez-Dehesa, C. López, and J. Llinares, Phys. Rev. B **59**, 12169 (1999).
[5] T.-T. Wu, Z.-G. Huang, and S. Lin, Phys. Rev. B **69**, 094301 (2004).
[6] T.-T. Wu, Z.-C. Hsu, and Z.-G. Huang, Phys. Rev. B **71**, 064303 (2005).
[7] J. O. Vasseur, P. A. Deymier, B. Chenni, B. Djafari-Rouhani, L. Dobrzynski, and D. Prevost, Phys. Rev. Lett. **86**, 3012 (2001).
[8] M. Kafesaki, M. M. Sigalas, and N. Garcia, Phys. Rev. Lett. **85**, 4044 (2000).
[9] G. Wang, X. Wen, J. Wen, L. Shao, and Y. Liu, Phys. Rev. Lett. **93**, 154302 (2004).
[10] T.-T. Wu and Z.-G. Huang, Phys. Rev. B **70**, 214304 (2004).
[11] S. Benchabane, A. Khelif, J. Y. Rauch, L. Robert, and V. Laude, Phys. Rev. E **73**, 065601(R) (2006).
[12] J.-H. Sun and T.-T. Wu, Phys. Rev. B **74**, 174305 (2006).
[13] Y. Pennec, B. Djafari-Rouhani, J. O. Vasseur, A. Khelif, and P. A. Deymier, Phys. Rev. E **69**, 046608 (2004).
[14] J.-C. Hsu and T.-T. Wu, Phys. Rev. B **74**, 144303 (2006).
[15] A. Khelif, B. Aoubiza, S. Mohammadi, A. Adibi, and V. Laude, Phys. Rev. E **74**, 046610 (2006).
[16] F.-L. Hsiao, A. Khelif, H. Moubchir, A. Choujaa, C. Chen, and V. Laude, Phys. Rev. E **76**, 056601 (2007).
[17] B. Bonello, C. Charles, and F. Ganot, Appl. Phys. Lett. **90**, 021909 (2007).
[18] B. Morvan, A. Hladky-Hennion, D. Leduc, and J. Izbicli, J. Appl. Phys. **101**, 114906 (2007).
[19] S. Mohammadi, A. A. Eftekhar, A. Khelif, W. D. Hunt, and A. Adibi, Appl. Phys. Lett. **92**, 221905 (2008).
[20] T.-T. Wu, Z.-G. Huang, T.-C. Tsai, and T.-C. Wu, Appl. Phys. Lett. **93**, 111902 (2008).
[21] Y. Pennec, B. Djafari-Rouhani, H. Larabi, J. O. Vasseur, and A. C. Hladky-Hennion, Phys. Rev. B **78**, 104105 (2008).
[22] COMSOL MULTIPHYSICS 3.3 Manual, Comsol AB, Stockholm, Sweden.
[23] We use the elastic constants $c_{11}=111$ GPa, $c_{12}=61$ GPa, $c_{44}=25$ GPa, and mass density $\rho=2695$ kg/m^3 for aluminum 6061.
[24] V. Laude, L. Robert, W. Daniau, A. Khelif, and S. Ballandras, Appl. Phys. Lett. **89**, 083515 (2006).
[25] T.-T. Wu and Y.-H. Liu, Ultrasonics **37**, 23 (1999).
[26] T.-T. Wu and J.-S. Fang, J. Acoust. Soc. Am. **101**, 330 (1997).
[27] F. Hsiao, A. Khelif, H. Moubchir, A. Choujaa, C. Chen, and V. Laude, J. Appl. Phys. **101**, 044903 (2007).